Effect of Thread Milling Penetration Strategies on the Dimensional Accuracy

Guillaume Fromentin[a], Vishal S Sharma[a,b], Gérard Poulachon[a], Yann Paire[a], Romain Brendlen[a]
[a]Arts et Metiers Paris Tech, LaBoMaP, 71250 Cluny, France
[b]Dept. of Industrial & Production Engg, National Institute of Technology, Jalandhar-144011, India

Abstract

Day by day the application of thread milling process is enhancing in industry because of its inherent advantages over other thread cutting techniques. The current study dwells on the interference issue, which is generated during thread milling. It was observed that there are two sources of interference on the thread produced i.e interference induced during mill penetration and during full machining. This interference leads to an overcut on the thread, thus it produces dimensionally inaccurate thread. The interference produced by penetration is much more as compared to interference generated during full machining of thread. Thus, there is a pressing need to analyze interference during penetration. So this study evaluates different applied penetration strategies and the level of interference produced. Further, the study suggests modified penetration strategies in order to reduce the interference produced and hence create more accurate thread. This investigation is supported by analytical modeling and experimental exploration.

Keywords

Thread milling, interference, dimensional accuracy, penetration strategies

Nomenclature

Abbreviations

CNC: Computer numerical control

FM: full machining

HRP: half revolution penetration

MHRP: modified half revolution penetration

MQRP: modified quarter revolution penetration

PS: penetration strategy

QRP: quarter revolution penetration

SP: straight penetration

Referential and parameters

$R_o = (o_1, \mathbf{e_1}, \mathbf{e_2}, \mathbf{e_3})$ referential linked to the mill with $\mathbf{E_3} = \mathbf{e_3}$ and angle $(\mathbf{E_1}, \mathbf{e_1}) = \Theta$

$R_O = (O_1, \mathbf{E_1}, \mathbf{E_2}, \mathbf{E_3})$ referential linked to the thread $(O_1, \mathbf{E_3})$: hole axis

z_{ce}: altitude of a cutting edge point in the R_o referential

Θ: angular position of the mill

θ_1: angular position of the mill axis with reference to O_1 point

θ_2: angular position of the mill axis with reference to O_2 point

θ_S: cross section angle

Thread characteristics

D: nominal diameter of the internal thread (mm)

D_1: minor diameter of the internal thread (mm)

D_2: pitch diameter of the internal thread (mm)

$E_{r\,max}(\theta_S)$: maximum radial error in θ_S cross section (μm)

$E_{r\,max}$: maximum radial error (μm)

$E_{r\,max1}$: maximum radial error in S1 cross section (μm)

$E_{r\,min}$: minimum radial error (μm)

$E_{r\,min1}$: minimum radial error in S1 cross section (μm)

E_r: radial error (μm)

P: thread pitch (mm)

p: angular thread pitch (mm/rad)

Computing parameters

D_{2m}: mill pitch diameter (mm)

D_m: mill diameter (mm)

ES_{ME} (θ_i, z_{ce}): envelope surface of mill envelope i ∈ {1, 2}, 1 = full machining, 2 = penetration

GTP (θ_s, z_{ce}): generated thread profile

MC (θ_i): mill center trajectory, i ∈ {1, 2}

MC_3 : 3rd component of mill center trajectory

ME (Θ, θ_i, z_{ce}): mill envelope i ∈ {1, 2}

MP (z_{ce}): mill profile

NTP (θ_s, z): nominal thread profile

NTS (θ_s, z): nominal thread surface

R(θ): rotating operator $\mathbf{R}(\theta) = \begin{bmatrix} \cos(\theta) & \sin(\theta) & 0 \\ -sin(\theta) & \cos(\theta) & 0 \\ 0 & 0 & 1 \end{bmatrix}$

R_{mc}: helix radius of the mill center trajectory for full machining (mm)

R_{mcp}: helix radius of the mill center trajectory for penetration (mm)

$R_{ES_{ME}}(\theta_s, z_{ce})$: radius of envelope surface for mill envelope

r_p: radial penetration (mm)

ΔZ: Z-axis variation of the mill during penetration/FM (mm)

Ψ: Inclination angle of mill center trajectory

1. Introduction

Threaded parts are needed for wide applications in engineering industry as they are used for fastening and/or converting rotatory motion to linear. There are many ways of categorizing threads like internal or external, based on the form (square, triangular, trapezoidal or other shapes) and type of handedness (left or right). Each thread is characterised by nominal diameter, pitch, number of starts and other parameters. They have been standardized in early nineteenth century in order to facilitate compatibility between different manufacturers and users. The methods of producing threads include thread tapping, thread forming and thread grinding. Most of external threads are rolled and internal threads are tapped, but today they can also be milled because of modern machine tool technology (CNC). A thread milling tool is needed for this operation. Such milling cutters are almost all-purpose tools as the same tool can be used to produce a variety of thread diameters or tolerances with the same thread pitch. Blind hole, through hole, internal and external threads can be milled in materials that produce long or short chips. High-speed cutting is also possible with thread milling [1, 2].

As compared to tapping, in thread milling, it is easier to evacuate broken tool from the part without damaging it. This is quite advantageous in case of high cost parts as frequently used in aerospace industry. The thread milling process needs less torque as compared to tapping for large thread diameters. The limitation associated with the process is that it is slower than tapping and requires a 3-axis CNC machine for execution.

Threaded joints are extensively used in mechanical engineering firms for different applications so they must satisfy a variety of operating requirements. Hence it becomes necessary to manufacture threads of various accuracies [3]. It is also shown that precision manufacturing of the screw threads enhances the mechanical properties of high-strength bolts [4]. A few researchers have reported about precision and surface integrity of threads produced by tapping [5-7]. Some researchers have also investigated on cutting force modeling in tapping [8] and in thread milling [9]. Moreover, a study was also reported on a simplified two-dimensional numerical simulation method for form grinding the thread [10]. Recently interference issue has been dealt quite systematically for 5-axis machining by the researchers [11]. To the best knowledge of the authors, not much has been reported on the accuracy of threads produced by thread milling. This fact advocates the need for exploration in this area.

The objective of this study is to develop thread milling interference models and conduct experimental exploration that could be used to understand underlying reasons for interference that leads to dimensional errors on the thread. Furthermore, the paper also proposes various methods for enhancing the accuracy of the thread produced. The article is organized as follows: section 2 provides a brief background of the thread milling process. Section 3 discusses the model for estimation of errors produced. Thereafter section 4 & 5 elaborate experimental investigation, model validation and more peculiarities.

2. Brief Background of thread milling

Thread milling is a process that produces threads by the rotation of the milling cutter and the synchronous movement of the three main axes of the machine tool. There are six steps followed in thread milling, as shown in Fig. 1. In the first step, the thread milling cutter gets in line with the hole axis, this step is named as "infeed". Then, the mill moves into the hole up to the programmed depth, this step is termed as "axial setting to thread depth". The third step is an entry loop in which the tool radially enters into the part, called "penetration". Here the tool also moves up i.e. in Z-axis equal to half of the thread pitch (for half revolution penetration) since it is a right hand thread produced by down milling mode [12]. The fourth step is referred to as "full machining" in which the thread milling is carried out in a 360° helical movement of the mill. In this step also the tool travels in Z-axis but equal to thread pitch. Thereafter in the fifth step, the tool moves away from the part, using the same strategy as was used during penetration, this step is named as "retraction". In this step, the tool moves up in Z-axis by an amount equal to half of the thread pitch. In the sixth step, the mill is taken out of part and is termed as "thread completed".

The penetration strategies (PS) used in the study are straight penetration (SP), half revolution penetration (HRP) and quarter revolution penetration (QRP) (refer Fig. 2). In SP, the mill engages with the part following a straight line trajectory. There is no Z-axis displacement during this movement. For HRP, the tool follows a half-helical path to engage with the part, during this movement, it also travels equal to P/2 in Z-axis. QRP utilizes quarter helical trajectory for engagement with the part and P/4 movement in Z-axis. HRP and QRP strategies are employed in industry while the SP strategy is considered for comparisons with them.

Thread milling is a specific technique to produce threads, nevertheless with this, there exists a geometrical problem to obtain desired final surface like for other techniques. The use of milling or of grinding with form tools for machining sculptured surfaces, worm threads,

grooves, flutes or helical gears leads to geometrical errors, named interference. It can be an overcut (too much material is removed) or undercut (not enough material is removed) [11]. In the thread milling process, two aspects are of major concern i.e precision of the thread produced and cutting forces generated. This article addresses the issue of precision of threads produced. It has been proved that full machining of threads leads to interferences and these errors can be corrected by changing tool position during machining and/or by adapting tool profile [13]. During the course of the current study, the errors induced due to penetration strategies have been recognized and dealt with.

3. Modeling of interference

In this section, modelling for interference is discussed which makes use of surface based approach. Figure 2 defines the parameterization of the internal thread milling for FM and penetration strategies (SP, HRP, QRP). For thread milling operation, the penetration and the retraction trajectories are same, thus they share same set of equations and conditions. So the computations for interference in this study were carried out for penetration and FM. Internal threads were dealt here because it represents the majority application of thread milling. Further external thread milling induces minor problems of interference. It was decided to focus on right hand metric threads produced by down milling mode. The reason for this selection was, producing left hand or right hand threads generates the same level of interference. The various computations were carried out on Mathematica software and the flow chart is shown in Fig. 3.

The algorithm starts with inputting nominal thread diameter (D), thread pitch (P) of the internal thread and mill diameter (D_m) for the thread milling cutter. Then, it computes minor diameter (D_1), pitch diameter (D_2), nominal thread profile (**NTP**), nominal thread surface (**NTS**) for the thread. At the same time it also calculates mill pitch diameter (D_{2m}) and mill profile (**MP**) for the thread milling cutter. Then, it calculates mill center trajectory (**MC**) based upon whether it is FM, HRP or QRP. Thereafter mill envelope (**ME**), envelope surface of mill envelope ($\mathbf{ES_{ME}}$), generated thread profile (**GTP**) are calculated. Finally radial error (E_r) is computed.

3.1 Thread and mill profiles

The nominal thread profile (**NTP**) is a thread profile which is to be produced after machining as per ISO standard [14]. It is defined by six points joined by lines in (O_1, **E_1, E_3**) referential as in [13]. Then, the nominal thread profile (**NTP**) is parameterized by Eq. (1). The nominal thread surface (**NTS**) is defined as a function of the nominal thread profile (**NTP**) and is given by Eq. (2) (refer Fig. 4 & 5).

$$\mathbf{NTP}(\theta_s,z)=\begin{bmatrix}\mathrm{NTP}_r(z)\\ z\end{bmatrix}+\begin{bmatrix}0\\ p.\theta_s\end{bmatrix}\quad 0<z<P \quad \ldots (1)$$

$$\mathbf{NTS}(\theta_s,z)=\begin{bmatrix}0\\ 0\\ p.\theta_s\end{bmatrix}+\mathbf{R}(\theta_s).\begin{bmatrix}\mathrm{NTP}_r(z)\\ 0\\ z\end{bmatrix}\quad 0<z<P \quad \ldots (2)$$

The maximum diameter of mill is defined by D_m. Mill profile (**MP**) is also defined by six points joined by lines as a function of altitude of a cutting edge point (z_{ce}) in the R_o referential as in [13] and is given by Eq. (3).

$$\mathbf{MP}(z_{ce})=\begin{bmatrix}\mathrm{MP}_r(z_{ce})\\ z_{ce}\end{bmatrix}\quad 0<z_{ce}<P \ldots (3)$$

3.2 Definition of mill centre trajectories

The thread is produced when the mill moves along the mill centre (**MC**) in a circular helix during FM. Its radius (R_{mc}) is obtained by the radial offset which is reqired to superimpose the pitch line of two profiles (**NTP** and **MP**) as shown in Fig. 2a and Fig. 5. This condition is represented by Eq. (4). The equations 4 to 18 are mentioned in Table 1. The mill center trajectories (**MC**) for various cases are also expressed in Table 1. The mill center trajectory (**MC**) for FM is given in Eq. (5). Referring Fig. 2c coordinates of O_2 point for HRP is given in Eq. (6). The helix radius (R_{mcp}) and mill center trajectory (**MC**) for HRP are expressed by Eq. (7) and Eq. (8) respectively in the R_o referential. The solution provided by Eq. (8) is a circular helix so it can be programmed using G02/G03 NC codes. Subsequently in the experimental investigation it shall be shown that HRP strategy generates more interference than FM. So a modified half revolution penetration (MHRP) approach is proposed considering θ_1 angle for computing axial movement (Eq. 9). The relationship between the θ_1 and θ_2 angles is given by Eq. (10). The Z-axis component (MC_3) values of mill centre trajectory for HRP and MHRP (case B: Table 3) are indicated in Fig. 6a. It can be seen that there are different Z-axis (MC_3) values for the HRP and MHRP thus they would generate different levels of interference. It shall be shown subsequently that MHRP generates low

level of interferences as compared to HRP and FM. MHRP ensures same inclination angle (Ψ) of mill centre trajectory (**MC**) for penetration and FM.

Furthermore, in case of QRP, there is also mismatch of the inclination angle (Ψ) of mill centre trajectory (**MC**) for penetration and that for FM. The coordinates of O_2 point for QRP are given in Eq. (11). Referring Fig. 2d, helix radius penetration (R_{mcp}) and mill center trajectory (**MC**) for QRP are expressed by Eq. (12) and Eq. (13) in the R_o referential. The solution provided by Eq. (13) is circular helix so it can be programmed using G02/G03 NC codes. QRP strategy generates more interference as shall be shown further, so first modified quarter revolution penetration ($MQRP_1$) approach is proposed and it is given by the Eq. (14). The relationship between the two angles (θ_1 and θ_2) is given by Eq. (15). The solution is by substituting θ_1 angle from Eq. (15) in Eq. (14). This solution is a not a circular helix so it cannot be programmed using G02/G03 NC codes. Nevertheless there exists a special case for first modified quarter revolution penetration ($MQRP_{1S}$) strategy in which the solution is a circular helix. The case becomes special when $R_{mc} = 2P$, then $\theta_1 = \theta_2/2$. So by substituting θ_1 angle from Eq. (16) in Eq. (14) provides the solution which is circular helix. It is interesting to note that the solution provided for $MQRP_{1S}$ is also same as that for MHRP.

$MQRP_1$ solution which is not a circular helix, can be implemented by dividing path into many small linear segments, and then, writing NC program. But this process will make program more cumbersome and time consuming therefore difficult to implement. So a linear approximated solution $MQRP_2$ is proposed as given by Eq. (14). This solution is obtained by substituting θ_1 angle from Eq. (17) in Eq. (14). This proposed solution is quite easy to implement on CNC machine using G02/G03 NC codes The $MQRP_2$ solution respects variation of thread altitude (ΔZ) between the start and end points of penetration as shown in Fig. 6b. Further, another formulation for the modified quarter revolution strategy is provided by $MQRP_3$ given in Eq. (18). Here the developed helices of mill centre trajectory (**MC**) at penetration and for FM have the same slope along the trajectory. It can be seen in Fig. 6b that $MQRP_3$ solution respects the thread altitude only at the end point. For the special case where $R_{mc} = 2P$, there $MQRP_1$, $MQRP_2$ and $MQRP_3$ strategies have identical formulations, i.e. circular helix, as represented by case C in Table 4.

3.3 Calculation of mill envelope

The mill envelope (**ME**) is the surface obtained by the revolution of the mill profile (**MP**) around the mill axis. The surface of the mill envelope (**ME**) can be analytically formulated by

Eq. (19). which is in R_O referential. For right hand threads, because of the helix angle of the nominal thread surface (**NTS**), the mill envelope (**ME**) crosses the upper flank of the nominally defined thread surface in front of $\theta_s = \theta_1$ cross-section. Similarly it also crosses the lower flank, but from the opposite side of the $\theta_s = \theta_1$ cross-section (only for a specific mill position). This situation would reverse in case of left hand threads. Hence there is interference, which is an overcut on the thread flanks (refer Fig. 4).

$$\boldsymbol{ME}(\Theta, \theta_i, z_{ce}) = \boldsymbol{MC}(\theta_i) + \boldsymbol{R}(\Theta).\begin{bmatrix} MP_r(z_{ce}) \\ 0 \\ z_{ce} \end{bmatrix} \text{ ... (19)}$$

i = 1 for full machining (FM) & i = 2 for penetration (HRP, MHPR, QRP, MQRP)

3.4 Interference Parameterization

In order to parameterize the generated thread profile (**GTP**), the envelope surface of mill envelope ($\mathbf{ES_{ME}}$) is calculated in 3D space. The envelope surface of mill envelope ($\mathbf{ES_{ME}}$) is obtained in Eq. (21) from the conditions formulated by Eq. (20).

$$det\left[\frac{\partial \mathbf{ME}}{\partial \theta_i} \quad \frac{\partial \mathbf{ME}}{\partial \Theta} \quad \frac{\partial \mathbf{ME}}{\partial z_{ce}}\right] = 0 \Leftrightarrow \Theta = \mathrm{f}_{\Theta}(\theta_i, \mathrm{z_{ce}}) \text{ .... (20)}$$

$$\boldsymbol{ES_{ME}}(\theta_i, \mathrm{z_{ce}}) = \mathbf{ME}(\theta_i, \mathrm{f}_{\Theta}(\theta_i, \mathrm{z_{ce}}), \mathrm{z_{ce}}) \text{ .... (21)}$$

Eq. (22) gives the value of the cross-section angle (θ_s) when envelope surface of mill envelope ($\mathbf{ES_{ME}}$) intersects it. The radius of envelope surface for mill envelope ($R_{ES_{ME}}$) is given by Eq. (23). Thereafter, generated thread profile (**GTP**) is obtained as indicated in Eq. (24). Finally, from the generated thread profile (**GTP**) and nominal thread profile (**NTP)** the radial error (E_r) is computed (refer Fig. 5).

$$\theta_s(\theta_i) = \arctan[\boldsymbol{ES_{ME}}(\theta_i, \mathrm{z_{ce}}).\boldsymbol{E_1}, \boldsymbol{ES_{ME}}(\theta_i, \mathrm{z_{ce}}).\boldsymbol{E_2}] \Leftrightarrow \theta_i = \mathrm{f}_{\theta_i}(\theta_s, \mathrm{z_{ce}}) \text{ .... (22)}$$

$$R_{\boldsymbol{ES_{ME}}}(\theta_s, \mathrm{z_{ce}}) = norm\begin{bmatrix} \boldsymbol{ES_{ME}}(\mathrm{f}_{\theta_i}(\theta_s, \mathrm{z_{ce}}), \mathrm{z_{ce}}).\boldsymbol{E}_1 \\ \boldsymbol{ES_{ME}}(\mathrm{f}_{\theta_i}(\theta_s, \mathrm{z_{ce}}), \mathrm{z_{ce}}).\boldsymbol{E}_2 \end{bmatrix} \text{.... (23)}$$

$$\boldsymbol{GTP}[\theta_s, \mathrm{z_{ce}}] = \begin{bmatrix} R_{\boldsymbol{ES\,ME}}(\theta_s, \mathrm{z_{ce}}) \\ \boldsymbol{ES_{ME}}(\mathrm{f}_{\theta_i}(\theta_s, \mathrm{z_{ce}}), \mathrm{z_{ce}}).\boldsymbol{E}_3 \end{bmatrix} \text{.... (24)}$$

4. Experimental exploration

The experimental study was undertaken in order to investigate effects of SP, HRP, QRP strategies on the accuracy of the thread produced. The analytical model described in the earlier section, is applied and results are compared with the experimental measurements. The

endeavour during the study was to observe the role of penetration strategies on the interference during thread milling. The planning for experimentation was done taking into consideration the cutting conditions mentioned in Table 2 and the experiments were conducted as per the Tables 3 & 4 for HRP and QRP respectively. The machine used for the experiments was a 3-axis vertical machining centre. The measurements of thread profiles were made on a mechanical scanning device. Aluminum alloy (AlCu4Mg) was opted for study as it exhibits good machinability characteristics and causes minimum tool wear. Solid carbide TiCN coated thread mills were used for the study. The experiments have been divided into eight cases (A to H) based upon nominal thread diameter (D), thread pitch (P) and mill diameter (D_m) combinations as shown in Tables 3 & 4. The nominal thread diameter (D) was equal to 20 or 32 mm, thread pitch (P) was 1 or 2 mm and mill diameter (D_m) was 10 or16 mm.

The first step in part preparation was to perform overall rough machining. Then, holes were prepared in the part with drilling tool and were enlarged with milling cutter using helical interpolation. The final hole size was obtained by boring operation. Finally the threads were produced by thread milling operation. The thread milling was carried out in two passes in order to have minimum tool deflection while cutting. For each case (A to H) one reference profile was created which was subsequently used for measurement of radial error (E_r). The reference profile is composed of grooves, which are produced in the part by straight penetration of the mill (completing radial penetration) followed by the peripheral movement along the hole using circular interpolation. There is no Z-axis movement during these stages, so grooves in the part are obtained without generating interference. Since there is no interference involved in producing the reference profile, thus it is assumed to be flawless (error free) and is used as reference for radial error (E_r) measurements. Radial error (E_r) is the error between machined thread scanned profile and the reference profile (refer Fig. 7). The radial error minimum ($E_{r\,min}$) is measured at the crest and the radial error maximum ($E_{r\,max}$) is measured at the root of the internal thread.

After completing the threading operations on all the parts, the threads were scanned on mechanical scanning device, which makes use of a stylus for measurements. The scanning on the part was done at two locations, S2 cross-section ($\theta_s = \pi$) and S1 cross-section ($\theta_s = 0$) as shown in Fig. 2a. S2 cross-section gives the radial error (E_r) caused by FM. S1 cross-section gives the radial error for FM and penetration, depending upon either of which is more. Then, the scanned reference profile was compared to each machined thread scanned profile and radial error (E_r) measurements were carried out (Fig. 7).

5. Discussions

The experiments were conducted and radial error (E_r) was measured. The discussions are organized as follows; first the results of FM are elaborated followed by HRP and QRP.

5.1 Interference for FM

Figure 8 evaluates factors affecting the radial error (E_r) for different cases during FM. One of the factors influencing radial error (E_r) is helix angle of the thread, which is a function of thread pitch (P) and nominal thread diameter (D). For the same nominal thread diameter (D) and mill diameter (D_m), the radial error (E_r) is less for lower thread pitch as indicated by cases A and C. Similarly keeping other parameters constant, the radial error (E_r) reduces with the increase in nominal thread diameter (D) as shown by cases A and B in the Fig. 8.

Another factor influencing interference is the ratio between mill diameter (D_m) and nominal diameter (D). It can be seen in Fig. 8 for cases A and E., with the same nominal thread diameter (D) and thread pitch (P), the radial error (E_r) reduces as the mill diameter (D_m) decreases. Further, for the same thread pitch (P) and mill diameter (D_m), the radial error (E_r) reduces as the nominal thread diameter (D) is increased as shown by cases A and B. Lower value of mill diameter (D_m) generates lower radial error (E_r) but the mill becomes delicate/fragile. Nevertheless in industry, the trend is to use mill diameter (D_m) close to minor diameter of the internal thread (D_1). For instance in case for thread where D = 16 mm, P = 2 mm (D_1 = 13.8 mm) the tool provider may propose D_m = 13.6 mm. This will lead to more interferences and hence loosing the accuracy of the thread produced.

A careful glance on the Fig. 8 for case A reveals that radial error ($E_{r\,max}$= 61.1 μm) is higher on the external diameter of the flank than on the internal one ($E_{r\,min}$ = 59.4 μm). This radial error ($E_{r\,max}$= 61.1 μm) for FM in case A can also be seen in Fig. 9a. For the ease of explanation, the radial error maximum ($E_{r\,max}$) values are used at appropriate places. The modelled radial error ($E_{r\,max}$ = 61.1 μm), generated by P_{m3} and P_{m4} points of the mill profile (**MP**) for FM shown in Fig. 10, indicates that these points generate same interference measured in any cross-section (θ_s= 0-2π).

Figure 12a and Fig. 12b indicate the result of comparisons for the computed and measured radial error ($E_{r\,max}$). The radial error ($E_{r\,max}$) for FM is observed in S2 cross-section (θ_s= π) and

it is indicated by "S2->FM" in Fig. 12. It can be seen that there is close match between computed and measured values of the errors for all the cases (A to H).

5.2 Interference for HRP

The maximum radial error ($E_{r\ max}$) for FM in case A is 61μm and for HRP is 139 μm (refer Fig. 9a). So in this case maximum radial error ($E_{r\ max}$) for HRP is more than half the tolerance interval ($T_{D2}/2$=106 μm) on D_2 flank diameter defined for thread 6 quality thread [15, 16]. Hence it is imperative to reduce the errors and bring them within the tolerance limits. The reason for more interference is that the axial movement to the mill is provided from O_2 point and not from the centre of the thread (O_1 point) so there is mismatch of the inclination angle (Ψ) of mill centre trajectory (**MC**) for penetration and that for FM. Hence the method for correcting this error is by providing the axial movement to the mill from the O_1 point and hence ensuring the same inclination angle (Ψ) of mill centre trajectory (**MC**) for penetration and FM.

In order to reduce the interferences, formulation named MHRP (as proposed in modeling section) was tested. It was found that MHRP (computed) induces less interference in S1 cross-section as compared to HRP and FM (refer Fig. 9a). Regarding the measurements, radial error (E_r) was measured at different points on the lower flank of the thread. The radial error (E_r) for FM can easily be measured at S2 cross-section ($\theta_s = \pi$). Furthermore, radial error (E_r) for HRP was measured at S1 cross section ($\theta_s = 0$). As it is more than the errors induced by FM, so it can also be measured easily. There is a close match between computed and measured results. The errors generated by MHRP are much less than that produced by FM, so it cannot be measured. The measurements at S1 cross-section ($\theta_s = 0$) will reflect the results of FM only. It can be seen in Fig. 9a that measured radial error (E_r) for MHRP also show results close to that of FM.

In order to extract more information about the process, the errors generated (modelled) by P_{m3} and P_{m4} points of the mill profile (**MP**) at different cross-sections are presented in Fig. 10a for FM, HRP and MHRP (Case A). FM generates same radial error ($E_{r\ max}$) for any cross-section values. It can be noted that the radial error ($E_{r\ max1}$ = 139μm) produced by points for HRP crosses the radial error ($E_{r\ max}$= 61μm) produced by FM, so penetration stragtegy induce more errors. For MHRP radial errors ($E_{r\ max}$) does not cross the radial errors ($E_{r\ max}$) produced by FM there by reducing the interferences during penetration. It is noteworthy that the P_{m3} and P_{m4} points produce different levels of errors when observed in different cross-

sections at a given instant. The radial errors ($E_{r\ max1}$) produced by P_{m3} and P_{m4} points are not maximum at S1 cross-section ($\theta_s = 0$). The maximum radial error ($E_{r\ max}$) produced by P_{m3} and P_{m4} points are at cross-section angles (θ_{sb} and θ_{sa}) respectively for MHRP. For case A, HRP affected 50˚ section of the thread. The radial error ($E_{r\ max1}$) measured in S1 cross-section ($\theta_s = 0$) for MHRP (case A) in Fig. 10a can also be observed in Fig. 9a. Similarly other radial errors in S1 cross-section ($\theta_s = 0$) indicated in Fig. 10a could also be observed in Fig. 9a.

The developed mill centre trajectory (**MC**) and its inclination angle (ψ) (refer Eq. (25): only for FM) for penetration and FM are shown in Fig. 11a.

$$\tan \psi = \frac{P}{2\pi R_{mc}} \ldots (25)$$

It can be seen that the inclination angle (ψ) for HRP strategy is double than that for FM (Fig. 11a). So there is a slope discontinuity between penetration helical trajectory and FM helical trajectory. Due to this difference of angles between two helical trajectories, there is more interference, which leads to overcut on the thread flanks. The proposed solution MHRP provides same angle for penetration and FM, so there is smooth matching between two helical trajectories. Hence the interferences are minimized and more accurate threads are produced.

Refering Fig. 12a there is also close match between the computed and measured radial error ($E_{r\ max1}$) for HRP. As HRP errors are more than that for FM so they are easily measurable at S1 cross-section ($\theta_s = 0$). The MHRP always produces errors less than that of FM so these cannot be measured at S1 cross-section ($\theta_s = 0$). The measurements at this cross-section will reflect errors produced by FM only (Table 3: column "error source in S1 cross section"). This is shown by "measurement affected by FM" in the Fig. 12a. Moreover, it can also be seen that SP produces less radial error ($E_{r\ max1}$) as compared to HRP for all cases.

5.3 Interference for QRP

Figure 9b represents the results of radial error (E_r) along the lower flank for FM, QRP and MQRP (case B). It can also be seen here that QRP (E_{rmax1} = 14.4 μm) generates more interferences than FM (E_{rmax} = 9.4 μm), this is similar to that was observed for HRP. Since radial error (E_r) for QRP was measured at S1 cross section (θ_s= 0) and it is more than the errors induced by FM, so it can be measured. Hence there is a close match between computed and measured results. As proposed in the modeling section, $MQRP_2$ should induce less interference, so it was implemented and compared to QRP and FM in Fig. 9b. The difference

between radial error (E_r) values for $MQRP_2$ and FM is quite small, so the measured radial errors (E_r) results are difficult to differentiate. But from the computed results it can be seen that $MQRP_2$ ($E_{r\ max1}$ = 9.1 μm) will generate interferences less than FM ($E_{r\ max}$ = 9.4 μm) in S1 cross-section (θ_s= 0). The error difference between two formulations ($MQRP_2$ and $MQRP_3$) was quite small and moreover it was difficult to measure small variations. Thus it was decided not the execute $MQRP_3$ solution experiments.

Figure 10b represents the modelled radial error ($E_{r\ max}$) generated by P_{m3} and P_{m4} points of the mill profile (**MP**) for FM, QRP and MQRP (case B). The radial error ($E_{r\ max1}$ = 14.4 μm) produced by QRP crosses the radial error ($E_{r\ max}$ = 9.4 μm) produced by FM, leading to more errors. It was also observed here that radial error ($E_{r\ max1}$) produced by P_{m3} and P_{m4} points are not maximum at S1 cross-section (θ_s = 0). Three formulations for MQRP are shown in the Fig. 10b. It can be seen that radial errors ($E_{r\ max}$) generated by $MQRP_1$ and $MQRP_3$ strategy do not cross the radial errors ($E_{r\ max}$) produced by FM thereby reducing the interference during penetration. But for $MQRP_2$ the radial errors ($E_{r\ max}$) cross slightly the radial errors ($E_{r\ max}$) produced by FM and hence leading to slightly more errors than FM (it is a linear approximate formulation). The maximum radial error ($E_{r\ max}$) produced by P_{m3} and P_{m4} points for $MQRP_2$ are at cross-section angles (θ_{sd} and θ_{sc}) respectively. The radial error ($E_{r\ max1}$ = 9.1 μm) measured in S1 cross-section (θ_s = 0) for $MQRP_2$ (case B) in Fig. 10b can also be observed in Fig. 9b. Similarly other radial errors in S1 cross-section (θ_s = 0) indicated in Fig. 10b could also be observed in Fig. 9b. Case C is a special one therefore the radial errors computed by various formulations ($MQRP_1$, $MQRP_2$ & $MQRP_3$) are the same.

Figure 11b shows inclination angle (ψ) for QRP strategy. Here also there is a difference between angles but it is less than that for HRP strategy. Referring Fig. 4b, the $MQRP_1$ trajectory is not a circular helix so it cannot be programmed using standard G02/G03 NC codes but error is minimized using this trajectory. So an approximate solution as given by $MQRP_2$ formulation is implemented. $MQRP_2$ gives almost same inclination angle (ψ) for penetration and FM, thereby reducing errors.

Figure 12b presents results of radial error ($E_{r\ max1}$ or $E_{r\ max}$) for experiments (case B to H) for SP, QRP and MQRP. It can be seen that QRP produces more interference than FM and they are reduced by $MQRP_2$ formulation. It is evident in Fig. 12 b that the radial error ($E_{r\ max1}$) is reduced with $MQRP_2$ strategy as compared to QRP experiments but these errors cannot be measured as they are less than or close to that produced by FM. This is shown by "measurement affected by FM" in the Fig. 12b. Next, referring Table 4 column "error source in S1 cross section", it can be seen that for two cases F and H, there is very small difference

between computed radial error (E_r) for FM and $MQRP_2$. So finally $MQRP_2$ is measured instead of FM. This happens only for two cases where difference between the errors was quite small so it may be omitted from the general trend observed for all other measured error cases. Both the solutions i.e $MQRP_2$ and $MQRP_3$ reduce interferences as compared to QRP, but $MQRP_3$ solution shall be slightly better than $MQRP_2$ as it follows path close to that of $MQRP_1$ (near the end). This is also in line with the findings of the Fig. 10b where $MQRP_3$ gives best results.

Further, it can be seen here that SP produces less radial error ($E_{r\ max1}$) as compared to QRP for all cases. For SP the engagement angle of mill teeth is more as compared to QRP. So it may lead to higher cutting forces, which in turn contribute to more tool deflection and therefore fewer overcuts on the thread flanks. Higher cutting forces may lead to the mill breakage if feed is not adapted during SP.

The characteristics summary for the different penetration strategies is presented in Table 5. In case of HRP, MHRP provides the best solution as it respects inclination angle (Ψ) and thread altitude. For QRP, $MQRP_1$ solution cannot be easily implemented on CNC machine as it is not a circular helix. The solutions, that can be easily programmed, are $MQRP_2$ and $MQRP_3$. Upon comparing these solutions, $MQRP_2$ provides almost same inclination angle (Ψ) for penetration and FM and it respects thread altitude at start and end point of penetration. The $MQRP_3$ solution provides same inclination angle (Ψ) for penetration and FM but it respects thread altitude only at end point of penetration. Nevertheless $MQRP_3$ solution follows a path close to that followed by $MQRP_1$ (which provides best solution) near the end of penetration. Thus $MQRP_3$ provides a slightly better solution than $MQRP_2$.

Further, regarding which applied penetration strategy (HRP or QRP) generates less interference, investigation reveals that QRP generates less radial errors (E_r), except for case C ($MQRP_{1S}$: Special case) where it remains equal. This implies that QRP strategy should induce less interference as compared to HRP strategy. Further on comparing the radial errors (E_r) produced by MHRP and MQRP, it was observed that for all cases (except case C: $MQRP_{1S}$), MHRP produces less errors. So it can be concluded that for all the cases studied MHRP will generate minimum errors and hence produce most accurate threads.

Regarding the measurement results, by and large there is close match between computed and measured radial errors (E_r) for all cases of FM, HRP and QRP. As MHRP, MQRP formulations generate errors less than or close to that of FM, which are not measureable in S1 cross-section. So finally errors for FM could only be measured in this cross-section. The possible reasons for slight deviations in the computed and measured values for different cases

could be the inevitable tool deflection and/or the inadvertent measurement errors. It may be noted that the computations were made by assuming no corner radius at the edge as this is a small region as compared to the flanks.

6. Conclusions

The process of thread milling leads to interference and so overcutting on the thread flanks. The conclusions of the study are given below:

- The factors influencing interferences during FM are thread helix angle and ratio between mill diameter and nominal thread diameter.
- HRP and QRP penetration strategies produce higher levels of interference as compared to FM.
- MHRP and MQRP strategies produce less interferences as compared to applied strategies i.e HRP & QRP.
- For reducing the level of interferences during penetration, MHRP and $MQRP_3$ are the most appropriate penetration strategies as they induce interferences less than that produced by FM.
- QRP strategy induces less interference as compared to HRP for applied PS where as MHRP strategy produces less interference as compared to MQRP for modified PS.
- SP does not induce more interference than the FM but it might lead to more cutting forces as the engagement angle of mill teeth is more as compared to HRP and QRP, so it is not employed.
- The analytical model computes the radial errors produced during penetration and full machining threads. Moreover, the analytical model is experimentally validated.

In order to produce accurate threads with thread milling, the first step is to use the right penetration strategy. Then, the second step is to reduce radials errors, induced during FM, by correcting radius of the mill center trajectory [13]. The modified half revolution penetration strategy generates minimum errors and hence produces most accurate threads. Further, a study could be initiated to investigate the cutting forces produced using different penetration strategies and investigate if the penetration strategies performing better from interference aspect are also best from cutting forces consideration.

Acknowledgements

The authors express their deepest gratitude towards Burgundy Council, France for providing financial support to carry out this research work in the form of a fellowship. The authors also acknowledge and express their sincere thanks towards M/s Walter Prototyp, Germany for providing cutting tools for the study.

References

1. Koelsch, J.R., 2005, "Thread milling takes on tapping," Manufacturing Engineer, 115, pp. 77-83.
2. Halas, D., 1996, "Tapping vs thread milling," Tooling and Production, 62, pp.99-102.
3. Ivanina, I. V., 2005, "Influence of parameters of the cutting part of taps on threading accuracy," Measurement Techniques, 48(10), pp. 990-994
4. Gerasimov V. Ya. and Gerasimova, O. V., 2009, "Influence of the accuracy of thread manufacture on the mechanical properties of high-strength bolts," Russian Engineering Research, ,29(4), pp. 345–347.
5. Mezentsev, O.A., DeVor, R.E. and Kapoor, S.G., 2002, "Prediction of thread quality by detection and estimation of tapping faults," Journal of Manufacturing Science and Engineering, 124, pp. 643-650
6. Fromentin, G., Poulachon, G., Moisan, A., Julien, B. and Giessler, J., 2005, "Precision and surface integrity of threads obtained by form tapping," CIRP Annals - Manufacturing Technology, 54(1), pp. 519-522.
7. Warrington, C. and Devor, R., 2005, "Experimental investigation of thread formation in form tapping, Journal of Manufacturing Science and Engineering, 127(4), pp. 829-836.
8. Armarego, E.J.A. and Chen, M.N.P., 2002, " Predictive cutting models for the forces and torque in machine tapping with straight flute taps, CIRP Annals - Manufacturing Technology, 51(1), pp.75-78.
9. Araujo, A.C., Silveira, J.L., Jun, M.B.G., Kapoor, S G. and Devor, R., 2006, "A model for thread milling cutting forces," International Journal of Machine Tools and Manufacture, 46(15), pp. 2057-2065.
10. Chiang, C.J., Fong, Z.H. and Tseng, J.T., 2009, "Computerized simulation of thread form grinding process," Mechanism and Machine Theory, 44(4), pp. 685-696.

11. Julien, C.J., Poulachon, G. and Duc, E., 2009, "New approach to 5-axis flank milling of free-form surfaces: Computation of adapted tool shape," Computer-Aided Design, 41(12), pp. 918-929.
12. Fromentin, G. and Poulachon, G., "Geometrical analysis of thread milling - Part 2: Calculation of uncut chip thickness," The International Journal of Advanced Manufacturing Technology, DOI: 10.1007/s00170-009-2401-4.
13. Fromentin, G. and Poulachon, G., "Modeling of interferences during thread milling operation," The International Journal of Advanced Manufacturing Technology, doi:10.1007/s00170-009-2372-5
14. ISO 68-1:1998 standard, ISO general purpose screw threads - Basic profile - Part 1: Metric screw threads.
15. ISO 965-1 standard, ISO general-purpose metric screw threads - Tolerances - Part 1: Principles and basic data.
16. ISO 965-2 standard, ISO general purpose metric screw threads - Tolerances - Part 2: Limits of sizes for general purpose external and internal screw threads - Medium quality.

Table 1: Mill center trajectories (**MC**) for FM, HRP and QRP

<table>
<tr><td colspan="3">Full machining (FM)</td></tr>
<tr><td colspan="3">$R_{mc} = \left(\frac{D_2 - D_{2m}}{2}\right)$....(4)</td></tr>
<tr><td>FM</td><td colspan="2">$\boldsymbol{MC}(\theta_1) = \begin{bmatrix} R_{mc}.cos\,\theta_1 \\ R_{mc}.sin\,\theta_1 \\ p.\theta_1 \end{bmatrix} \quad 0 < \theta_1 < 2\pi$ ....(5)</td></tr>
<tr><td colspan="3">Half revolution penetration (HRP)</td></tr>
<tr><td colspan="3">Coordinates of O_2 point: $\begin{bmatrix} \frac{R_{mc}}{2} \\ 0 \end{bmatrix}$....(6)</td></tr>
<tr><td colspan="3">$R_{mcp} = \frac{R_{mc}}{2}$....(7)</td></tr>
<tr><td>HRP</td><td>$\boldsymbol{MC}(\theta_2) = \begin{bmatrix} R_{mcp} \\ 0 \\ 0 \end{bmatrix} + \begin{bmatrix} R_{mcp}.\cos\theta_2 \\ R_{mcp}.\sin\theta_2 \\ p.\theta_2 \end{bmatrix}$ $-\pi < \theta_2 < 0$ ....(8)</td><td></td></tr>
<tr><td>MHRP</td><td>$\boldsymbol{MC}(\theta_2) = \begin{bmatrix} R_{mcp} \\ 0 \\ 0 \end{bmatrix} + \begin{bmatrix} R_{mcp}.\cos\theta_2 \\ R_{mcp}.\sin\theta_2 \\ p.\theta_1 \end{bmatrix}$ $-\pi < \theta_2 < 0$....(9)</td><td>$\theta_1 = \frac{\theta_2}{2}$....(10)</td></tr>
<tr><td colspan="3">Quarter revolution penetration (QRP)</td></tr>
<tr><td colspan="3">Coordinates of O_2 point: $\begin{bmatrix} P \\ 0 \end{bmatrix}$....(11)</td></tr>
<tr><td colspan="3">$R_{mcp} = R_{mc} - P$....(12)</td></tr>
<tr><td>QRP</td><td>$\boldsymbol{MC}(\theta_2) = \begin{bmatrix} P \\ 0 \\ 0 \end{bmatrix} + \begin{bmatrix} R_{mcp}.\cos\theta_2 \\ R_{mcp}.\sin\theta_2 \\ p.\theta_2 \end{bmatrix}$ $-\frac{\pi}{2} < \theta_2 < 0$....(13)</td><td></td></tr>
<tr><td>$MQRP_1$</td><td rowspan="3">$\boldsymbol{MC}(\theta_2) = \begin{bmatrix} P \\ 0 \\ 0 \end{bmatrix} + \begin{bmatrix} R_{mcp}.\cos\theta_2 \\ R_{mcp}.\sin\theta_2 \\ p.\theta_1 \end{bmatrix}$ $-\frac{\pi}{2} < \theta_2 < 0$....(14)</td><td>$\theta_1 = \arctan\frac{R_{mcp}.\sin\theta_2}{P + R_{mcp}.\cos\theta_2}$....(15)</td></tr>
<tr><td>$MQRP_{1S}$</td><td>$\theta_1 = \frac{\theta_2}{2}$....(16)</td></tr>
<tr><td>$MQRP_2$</td><td>$\theta_1 = \frac{2}{\pi}\arctan\left(\frac{R_{mcp}}{P}\right).\theta_2$....(17)</td></tr>
<tr><td>$MQRP_3$</td><td>$\boldsymbol{MC}(\theta_2) = \begin{bmatrix} P \\ 0 \\ 0 \end{bmatrix} + \begin{bmatrix} R_{mcp}.\cos\theta_2 \\ R_{mcp}.\sin\theta_2 \\ p.\left(\frac{R_{mcp}}{R_{mc}}\right)\theta_2 \end{bmatrix}$ $-\frac{\pi}{2} < \theta_2 < 0$....(18)</td><td></td></tr>
</table>

Table 2: Cutting conditions

Machine	Vertical 3-axis machining centre (Deckel Maho DMC 65V)
Mechanical scanning device	Surfascan 3D (Somicronic)
Stylus	Point radius 50 μm, Angle 30˚
Part Material	AlCu4Mg
Milling cutters specifications	D_m=10 mm, P= 2 mm ; D_m= 10 mm, P= 1 mm ; D_m=16 mm, P= 2 mm ; D_m= 16 mm, P= 1 mm ; All tools TiCN coated (Walter Prototyp make)
Type of milling	Down milling
Cooling condition	Flood coolant
Speed(V_c)	100 m/min
Feed per tooth (f_t)	0.05 mm/tooth
Depth of cut (ap)	10 mm

Table 3: Experiments for HRP

Ex. No	D (mm)	P (mm)	D_m (mm)	PS	Pene. comp. $E_{r\ max1}$ (μm)	FM comp. $E_{r\ max}$ (μm)	Meas. $E_{r\ max1}$ (μm)	Comp. $E_{r\ max}(\theta_s)$	Error source in S1 cross section
Case A									
A0	20	2	16	SP	x	61.2	58	x	FM
A1	20	2	16	HRP	139.1	61.2	134.2	140.8	HRP
A2	20	2	16	MHRP	34.0	61.2	56.9	61.2	FM
Case B									
B0	32	2	16	SP	x	9.5	6.1	x	FM
B1	32	2	16	HRP	25.4	9.5	26.3	28.5	HRP
B2	32	2	16	MHRP	6.3	9.5	8.5	9.5	FM
Case C									
C0	20	1	16	SP	x	15.2	13.2	15.2	FM
C1	20	1	16	HRP	34.0	15.2	29.1	34.4	HRP
C2	20	1	16	MHRP	8.5	15.2	10.0	15.2	FM
Case D									
D0	32	1	16	SP	x	2.4	1.6	x	FM
D1	32	1	16	HRP	6.3	2.4	6.3	7.1	HRP
D2	32	1	16	MHRP	1.6	2.4	2.8	2.4	FM
Case E									
E0	20	2	10	SP	x	15.2	15.3	x	FM
E1	20	2	10	HRP	40.7	15.2	40.9	45.8	HRP
E2	20	2	10	MHRP	10.1	15.2	14.3	15.2	FM
Case F									
F0	32	2	10	SP	x	4.3	5.8	x	FM
F1	32	2	10	HRP	13.2	4.3	11.5	18.1	HRP
F2	32	2	10	MHRP	3.3	4.3	5.0	4.3	FM
Case G									
G0	20	1	10	SP	x	3.8	1.3	x	FM
G1	20	1	10	HRP	10.1	3.8	10.0	11.4	HRP
G2	20	1	10	MHRP	2.5	3.8	3.9	3.8	FM
Case H									
H0	32	1	10	SP	x	1.1	0.6	x	FM
H1	32	1	10	HRP	3.3	1.1	3.6	4.5	HRP
H2	32	1	10	MHRP	0.8	1.1	1.0	1.1	FM

X: Not computed, Pene: Penetration, comp: Computed, Meas: Measured

Table 4: Experiments for QRP

Ex. No	D (mm)	P (mm)	D_m (mm)	PS	Pene. comp. $E_{r\ max1}$ (μm)	FM comp. $E_{r\ max}$ (μm)	Meas. $E_{r\ max1}$ (μm)	Comp. $E_{r\ max}(\theta_s)$	Error source in S1 cross section
Case A									
R_{mc}= P This case is not possible									
Case B									
B0	32	2	16	SP	x	9.5	5.4	x	FM
B1	32	2	16	QRP	14.5	9.5	14.0	15.8	QRP
B1*	32	2	16	$MQRP_1$	8.1	9.5	Δ	9.5	FM
B2	32	2	16	$MQRP_2$	9.2	9.5	11.0	9.7	FM
B3	32	2	16	$MQRP_3$	8.1	9.5	Δ	9.5	FM
Case C (Special case as R_{mc} = 2P)									
C0	20	1	16	SP	x	15.2	11.7	x	FM
C1	20	1	16	QRP	34.0	15.2	32.2	34.4	QRP
C1	20	1	16	$MQRP_1$	8.5	15.2	Δ	15.2	FM
C2	20	1	16	$MQRP_2$	8.5	15.2	12.5	15.2	FM
C3	20	1	16	$MQRP_3$	8.5	15.2	Δ	15.2	FM
Case D									
D0	32	1	16	SP	x	2.4	1.4	x	FM
D1	32	1	16	QRP	2.9	2.4	3.7	3.1	QRP
D1*	32	1	16	$MQRP_1$	2.2	2.4	Δ	2.4	FM
D2	32	1	16	$MQRP_2$	2.4	2.4	2.8	2.4	FM
D3	32	1	16	$MQRP_3$	2.2	2.4	Δ	2.4	FM
Case E									
E0	20	2	10	SP	x	15.2	16.5	x	FM
E1	20	2	10	QRP	31.7	15.2	30.9	35.5	QRP
E1*	20	2	10	$MQRP_1$	11.4	15.2	Δ	15.2	FM
E2	20	2	10	$MQRP_2$	12.4	15.2	17.0	15.3	FM
E3	20	2	10	$MQRP_3$	11.4	15.2	Δ	15.2	FM
Case F									
F0	32	2	10	SP	x	4.3	3.0	x	FM
F1	32	2	10	QRP	6.0	4.3	5.6	7.4	QRP
F1*	32	2	10	$MQRP_1$	4.0	4.3	Δ	4.3	FM
F2	32	2	10	$MQRP_2$	4.5	4.3	4.7	4.5	$MQRP_2$
F3	32	2	10	$MQRP_3$	4.0	4.3	Δ	4.3	FM
Case G									
G0	20	1	10	SP	x	3.8	3.1	x	FM
G1	20	1	10	QRP	5.3	3.8	5.6	5.7	QRP
G1*	20	1	10	$MQRP_1$	3.4	3.8	Δ	3.8	FM
G2	20	1	10	$MQRP_2$	3.8	3.8	4.2	3.9	FM
G3	20	1	10	$MQRP_3$	3.4	3.8	Δ	3.8	FM
Case H									
H0	32	1	10	SP	x	1.1	0.8	x	FM
H1	32	1	10	QRP	1.3	1.1	1.3	1.4	QRP
H1*	32	1	10	$MQRP_1$	1.0	1.1	Δ	1.1	FM
H2	32	1	10	$MQRP_2$	1.1	1.1	1.2	1.1	$MQRP_2$
H3	32	1	10	$MQRP_3$	1.0	1.1	Δ	1.1	FM

*: Not a circular helix; x: Not computed; Δ: Not measured; Pene: Penetration, comp: computed, Meas: Measured

Table 5: Characteristics summary for the different PS

PS	Solution	Radial error (E_r)	Thread inclination angle(ψ) respected	Thread altitude respect	Circular helix	Helix pitch	ΔZ
HRP	Used	Higher than FM	No	No	Yes	P	P/2
MHRP	Exact	Lowest	Yes	Yes	Yes	P/2	P/4
QRP	Used	Higher than FM	No	No	Yes	P	P/4
$MQRP_1$	Exact (general case)	Lowest of MQRP	Almost	Yes	No	ND	$\frac{P}{2\pi}.arctan\frac{R_{mcp}}{P}$
	Exact (special case)		Yes		Yes	P/2	P/8
$MQRP_2$	Approx.	Lower than FM	Almost	Yes only at start and end points	Yes	$\frac{2P}{\pi}.arctan\frac{R_{mcp}}{P}$	$\frac{P}{2\pi}.arctan\frac{R_{mcp}}{P}$
$MQRP_3$	Approx.	Lower than FM and $MQRP_2$	Yes	Yes only at end point	Yes	$\frac{R_{mcp}.P}{R_{mc}}$	$\frac{R_{mcp}.P}{4\,R_{mc}}$

ND: Not defined, Approx: Approximated

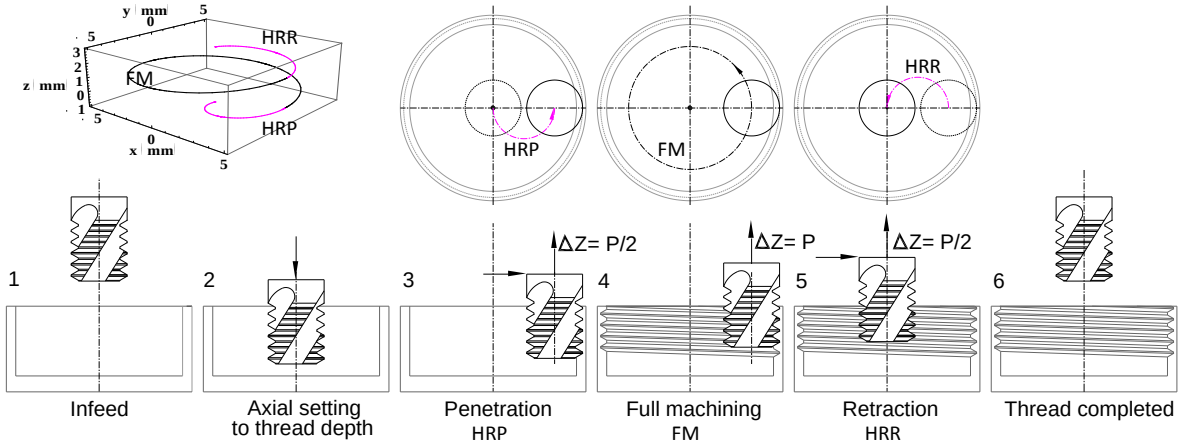

Fig. 1 Steps in thread milling cycle for HRP (right hand thread, down milling)

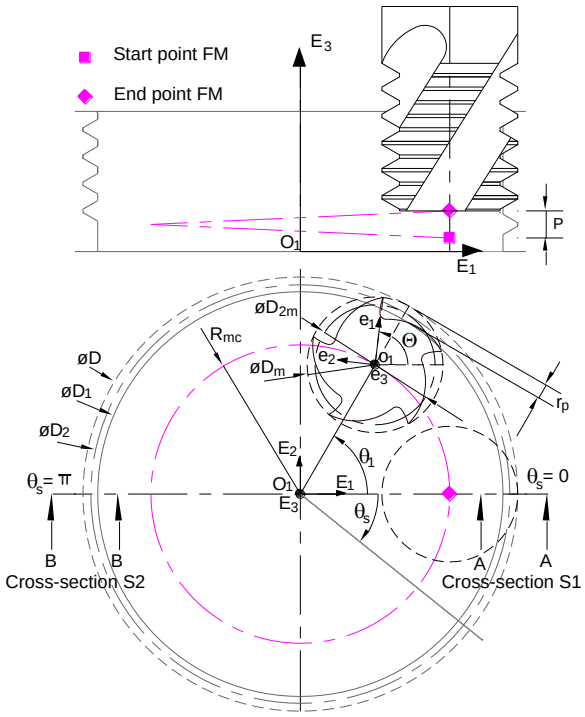

a: FM

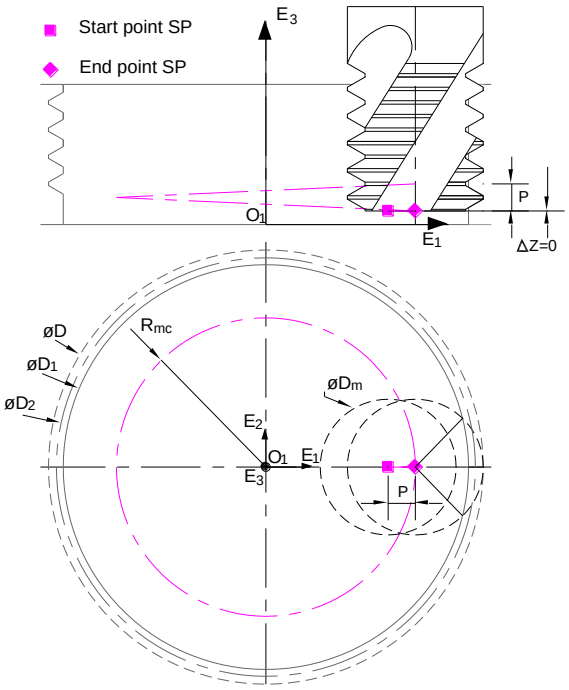

b: SP & FM

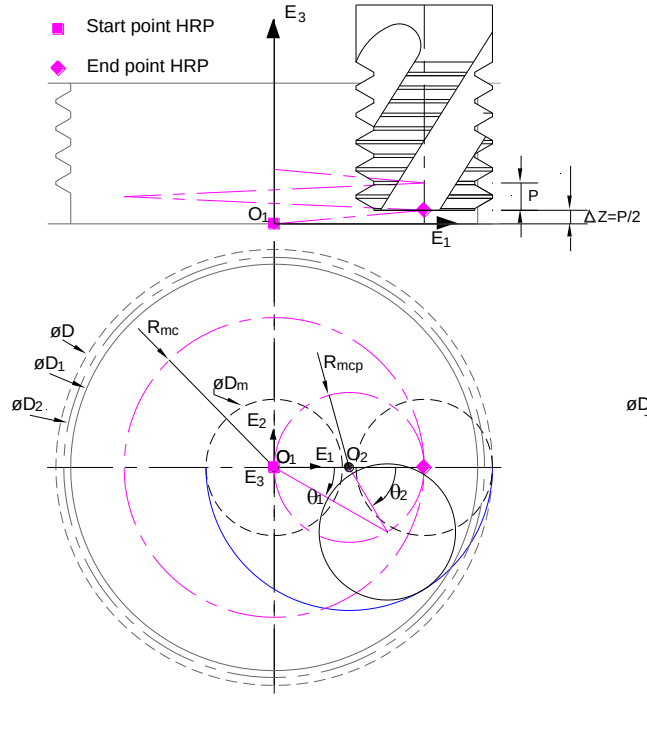

c: HRP & FM

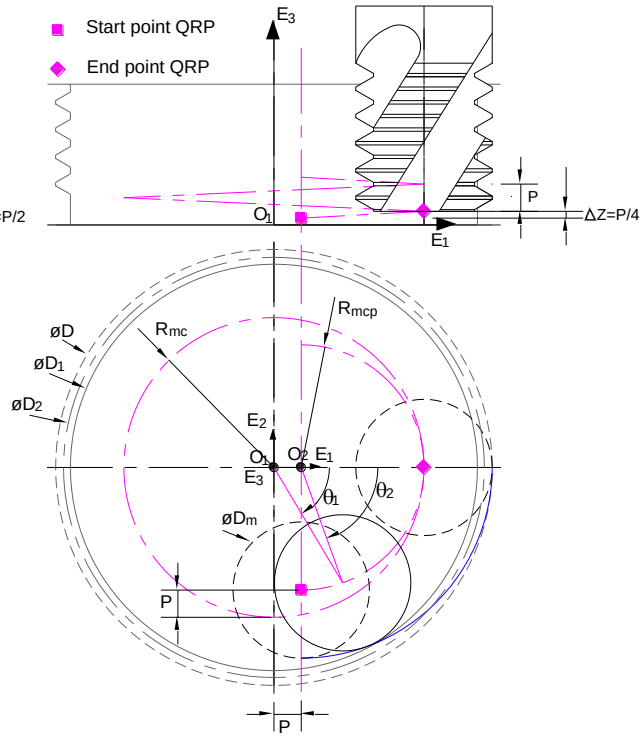

d: QRP & FM

Fig. 2 Thread milling parameterization for different strategies (case F)

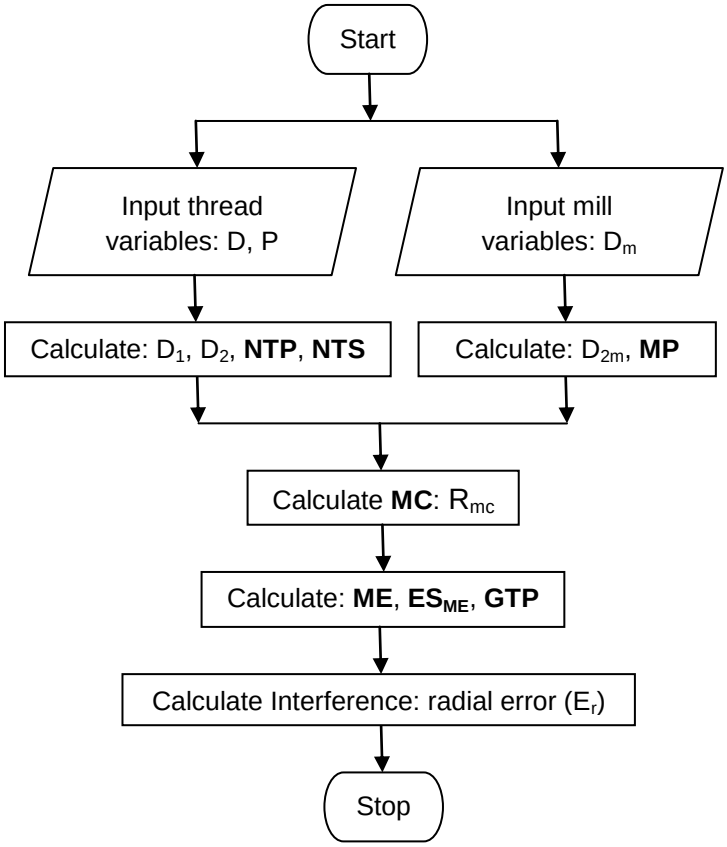

Fig. 3 Flow chart of the model

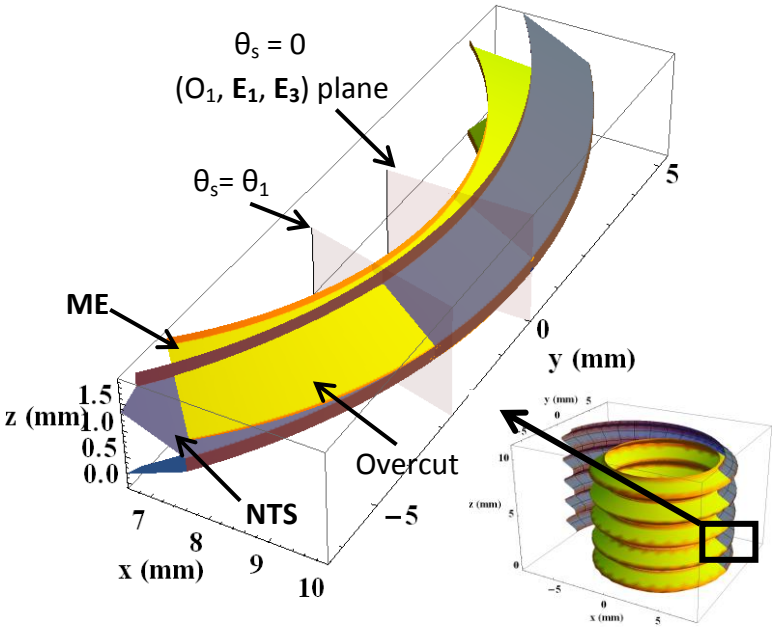

Fig. 4 Modelled nominal thread surface (**NTS**), mill envelope (**ME**) for FM in S2 cross-section (case A)

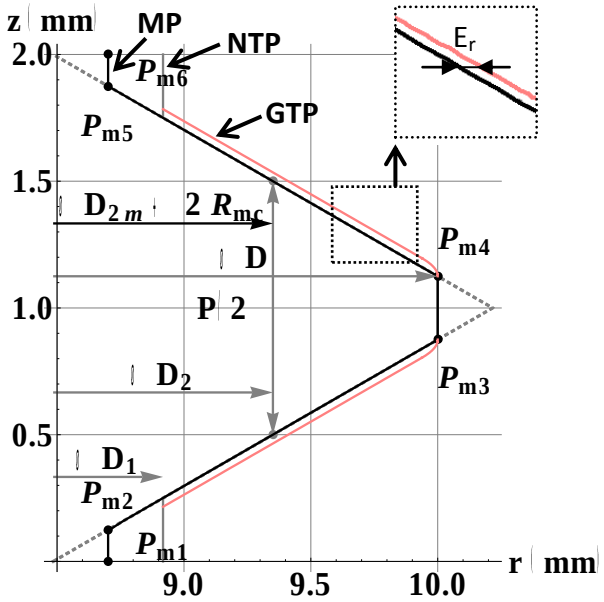

Fig. 5 Modelled generated thread profile (**GTP**) for FM in S1 cross-section (case A)

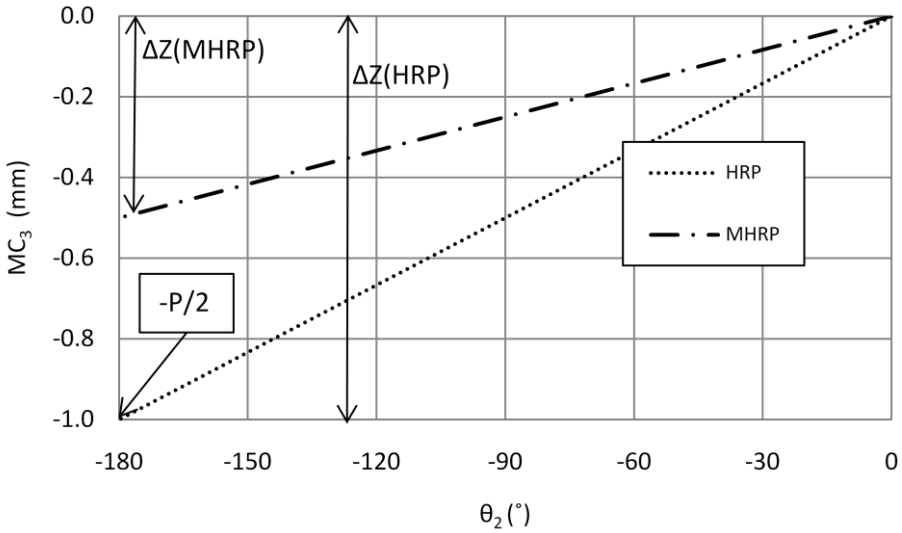

a

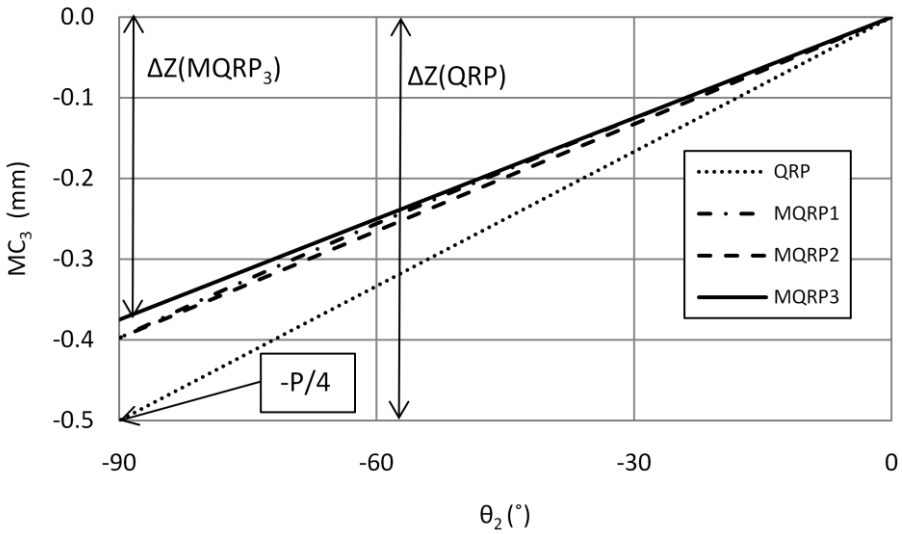

b

Fig. 6 Z-axis component (MC_3) of mill centre trajectory (case B)

a. HRP, b. QRP

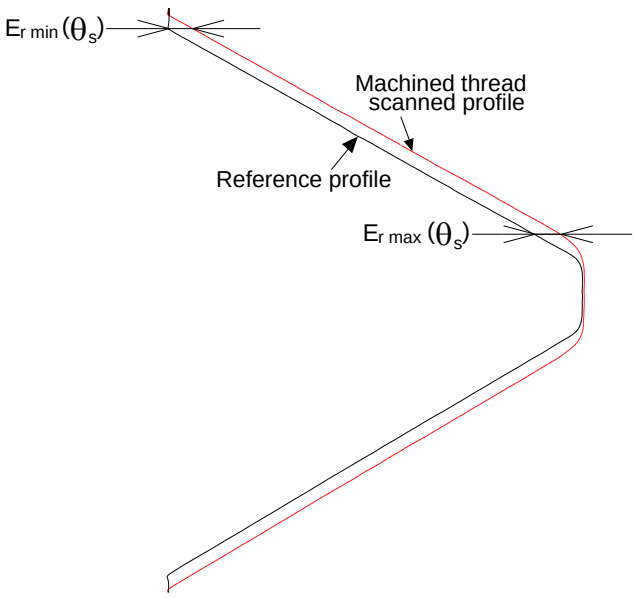

Fig. 7 Measured profiles & measurement of radial error in θ_s cross-section

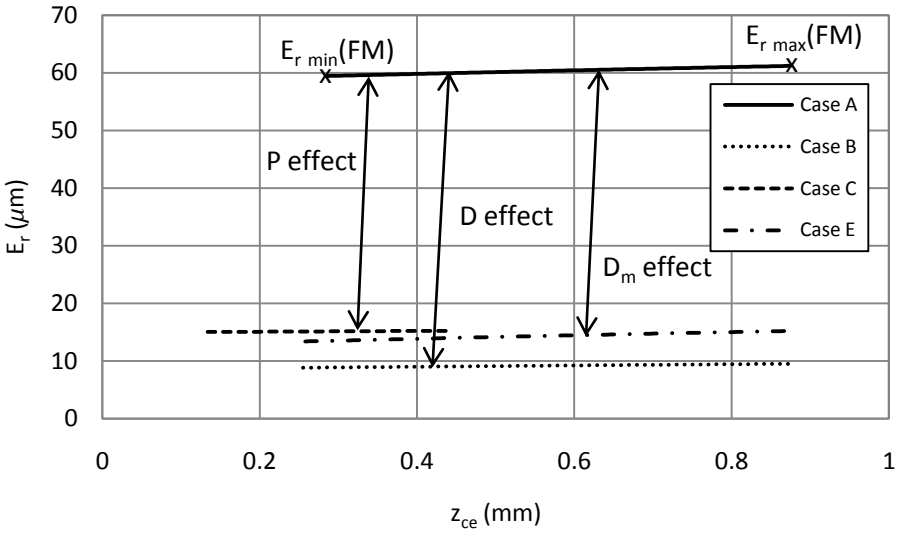

Fig. 8 Modelled radial error (E_r) along lower flank for FM

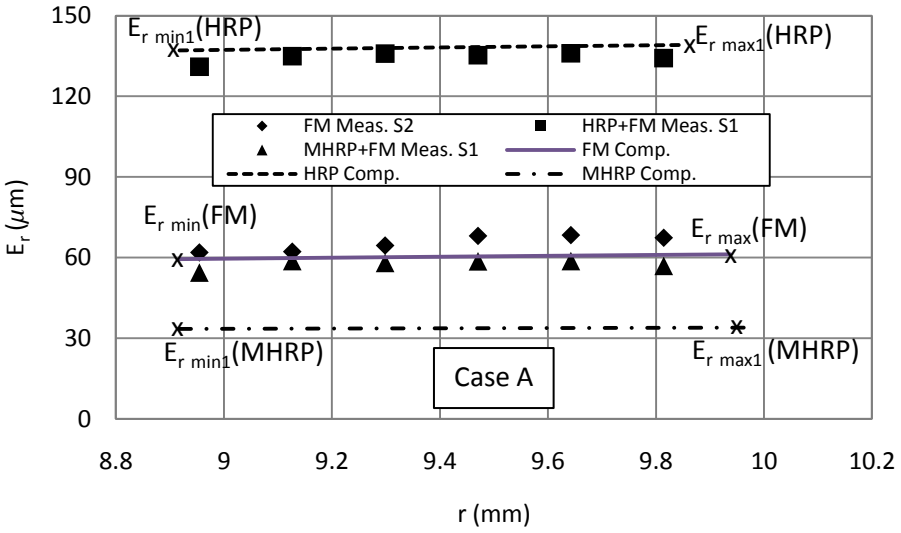

a

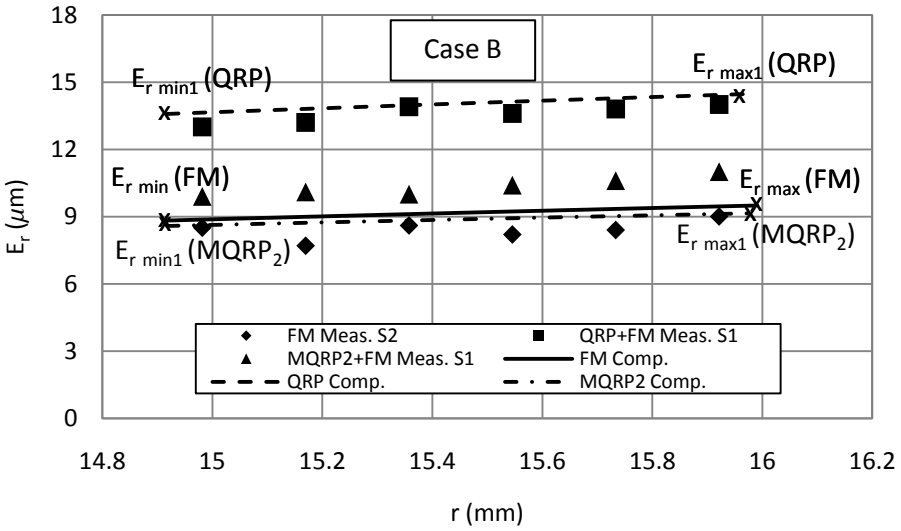

b

S1: measured in S1 cross-section, S2: measured in S2 cross-section

Fig. 9 Radial error (E_r) along lower flank

a. FM, HRP, MHRP; b. FM, QRP, $MQRP_2$

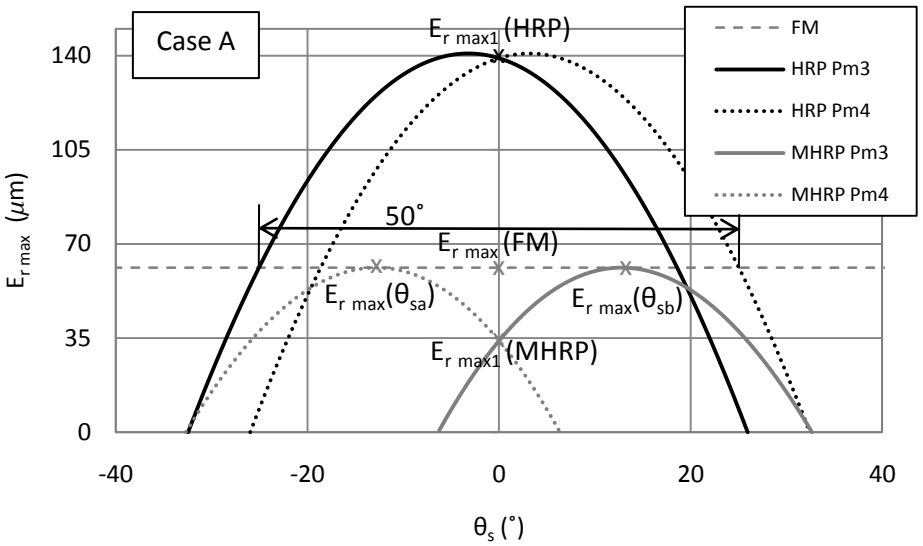

a

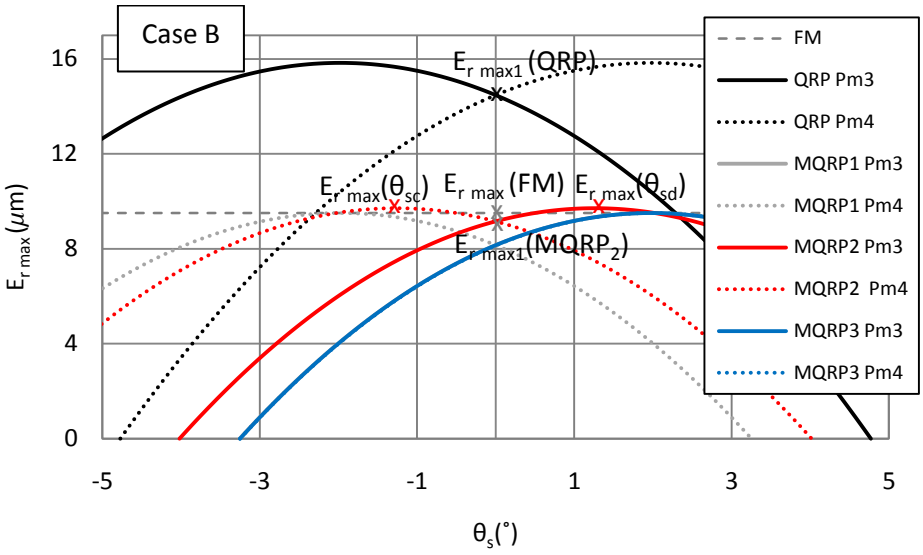

b

Fig. 10 Modelled radial error (E_r) generated by P_{m3} and P_{m4} points at different cross-sections a. HRP, b. QRP

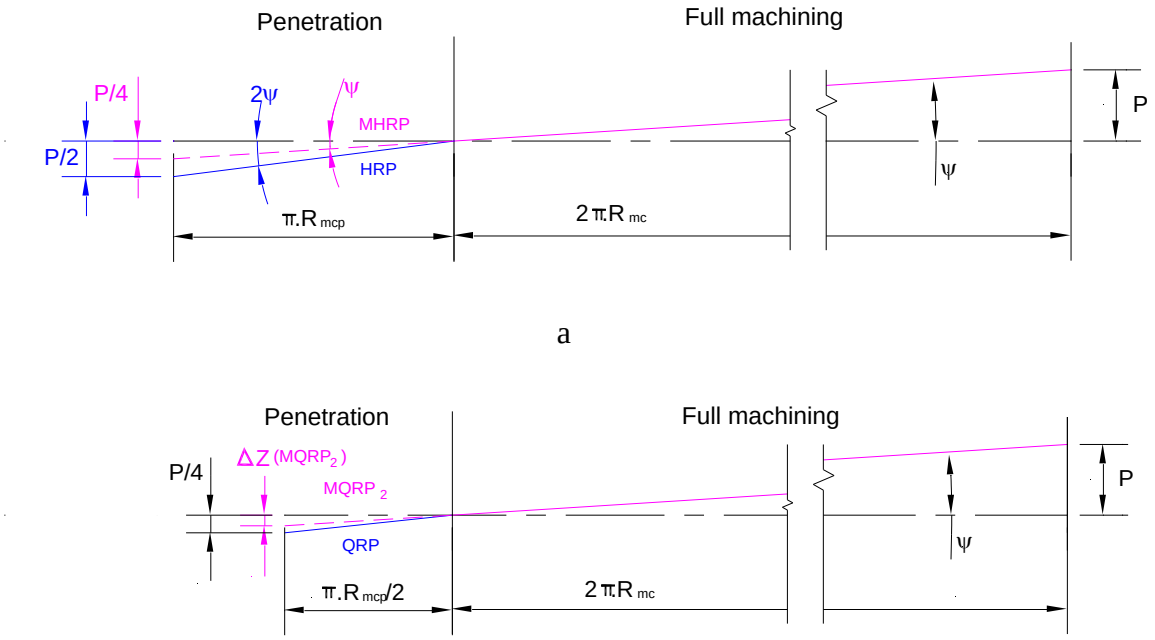

Fig. 11 Developed mill centre trajectory (**MC**) and its inclination angle (ψ) (Case E)
a. HRP, b. QRP

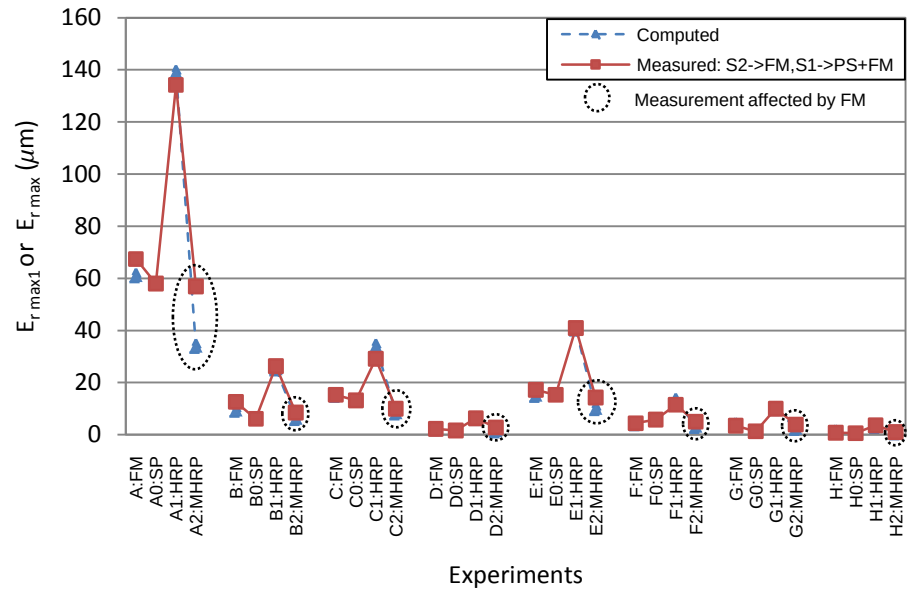

a

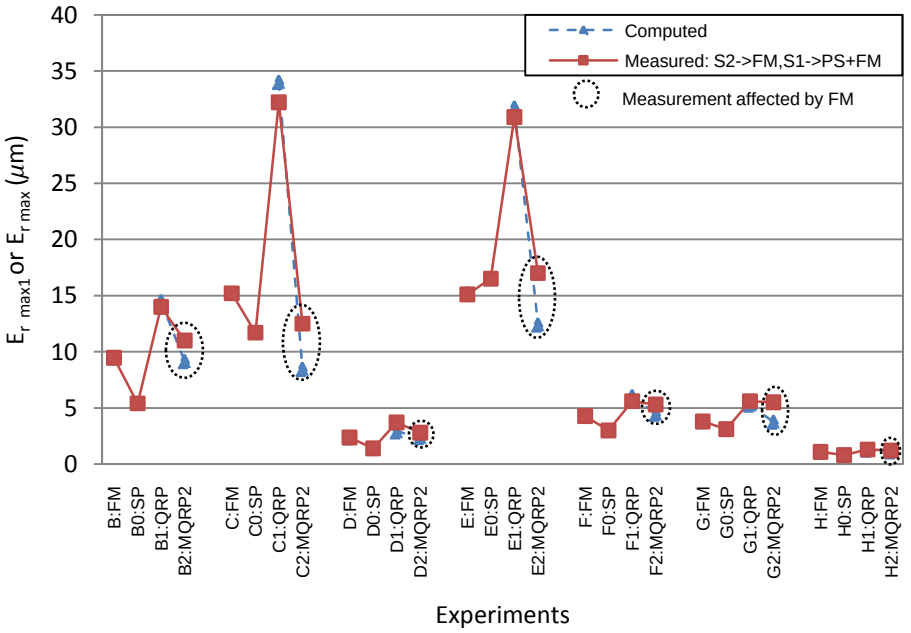

b

Fig. 12 Comparison of measured and computed radial error (E_r), a. HRP, b. QRP